ARCHIVES OF ELECTRICAL ENGINEERING VOL. 64(2), pp. 177-187 (2015)

DOI 10.1515/aee-2015-0015

Modelling of non-linear losses in an integrated contactless power supply for magnetically levitated elevator systems using discrete circuit elements*

ARYANTI KUSUMA PUTRI, RÜDIGER APPUNN, KAY HAMEYER

RWTH Aachen University, Institute of Electrical Machines
Schinkelstr. 4, 52056 Aachen, Germany
e-mail: aryanti.putri@iem.rwth-aachen.de

(Received: 14.10.2014, revised: 24.11.2014)

Abstract: A contactless energy transmission system is essential to supply onboard systems of electromagnetically levitated vehicles without physical contact to the guide rail. One of the possibilities to realise a contactless power supply (CPS) is by integrating the primary actuator into the guide rail of an electromagnetic guiding system (MGS). The secondary actuator is mounted on the elevator car. During the energy transmission, load dependent non-linear losses occur in the guide rail. The additional losses, which are caused by the leakage flux penetrating into the guide rail, cannot be modelled using the classical approach of iron losses in the equivalent circuit of a transformer, which is a constant parallel resistance to the mutual inductance. This paper introduces an approach for modelling the load dependent non-linear losses occurring in the guide rail using additional variable discrete circuit elements.

Key words: contactless energy transmission, electromagnetic guiding system, equivalent circuit model, ferromagnetic material at high frequency, magnetically levitated elevator, modelling of non-linear losses

1. Introduction

Electromagnetically levitated vehicles require a contactless power transmission to supply the onboard components in the moving part with electrical energy without sliding contacts or travelling cables. In a fast moving vehicle, e.g. maglev train, the power transmission is integrated within the drive, advantaging the harmonics produced from the propulsion device mounted to the guide rail [1]. On the contrary in a slow moving elevator system, a separate transmission system is required, since the aforementioned method is not feasible in low frequency operation. This yields further cost and space.

* This is extended version of paper which was presented at the 23th Symposium on Electromagnetic Phenomena in Nonlinear Circuits, Pilsen, Czech Republic 02-04.07.2014.

Previous studies to minimize cost and space are based on an integrated solution of guiding and power transmission, where the same flux path is used for both operations [2]. An alternative topology, where two different materials are used for the guiding and power transmission system, is proposed in [3]. The primary side consists of a soft magnetic actuator with coils around its lateral arms, which is integrated into the iron guide rail of a MGS. An identical secondary actuator is mounted on the elevator car. The nominal distance between the actuators d is 3 mm. The primary and secondary actuators have the same number of windings $N = 7$. When the position of primary and secondary actuators match, a power transmission is established and e.g. the battery supplying the onboard components on the elevator car can be charged. The working frequency of the CPS f_{CPS} is 25 kHz, which is much higher than the operating frequency range of the MGS ($f_{MGS} < 50$ Hz). Both of the systems are thereby decoupled. The described topology at aligned position and the flux density at no-load condition are illustrated in Figure 1.

By using a suitable reactive power compensation topology, an efficiency of more than 90% in the designed operating point of the CPS can be obtained. However, due to leakage flux paths penetrating the guide rail, load dependent additional losses occur in the system. These non-linear losses cannot be modelled utilizing the classic model of iron losses in a transformer, which is an equivalent parallel resistance to the coupling inductance. The other possibility to determine losses in the CPS is using specific iron losses at working frequency and flux density. However, the flux density in the guide rail of operating CPS cannot be measured and the modelled losses would be inaccurate. This paper presents a modelling approach of the non-linear losses using equivalent discrete circuit elements determined by measurements of uncompensated and compensated CPS.

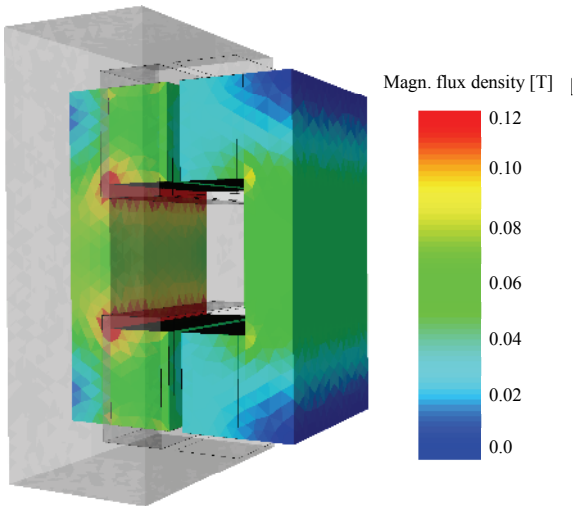

Fig. 1. The primary and secondary actuators of the CPS at aligned position with magnetic flux density at no-load operation (primary current $I_p = 10$ A)

2. Non-linear load dependent losses

The CPS topology proposed in [3] is constructed and measured. Through no-load measurements the inductance matrix **L**

$$\mathbf{L} = \begin{bmatrix} L_p & M \\ M & L_s \end{bmatrix}, \tag{1}$$

which consists of primary, secondary and mutual inductances (consecutively L_p, L_s, M), is determined. The values of the CPS equivalent circuit elements are listed in Table 1. Simulated and measured values show a good accordance with maximum deviation of 14.9% on primary inductance L_p, which means an increase in the primary side leakage flux $\Phi_{\sigma,1}$. The phase shift between voltage and current at no load is 86°, which shows a small deviation from the phase shift of an ideal CPS system (90°). Both indicate additional losses caused by the buried topology of the primary actuator. However, the losses are sufficiently small and can be neglected.

Table 1. Measured and simulated equivalent circuit components

	Simulated	**Measured**	**Deviation**
Primary self inductance L_p	47.75 µH	56.11 µH	14.9%
Secondary self inductance L_s	47.73 µH	52.18 µH	8.5%
Mutual inductance M	39.53 µH	38.7 µH	2.1%
Load Resistance R_{Load}	5 Ω	5.08 Ω	1.6%

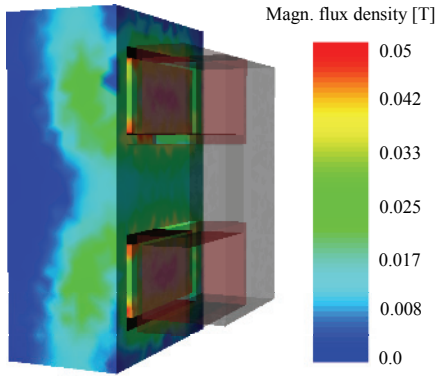

Fig. 2. Magnetic flux density within the guide rail in case of opposite currents applied to primary and secondary windings ($I_p = I_s = 10$ A)

From short circuit measurements a phase shift of 77° is observed. Due to the significant deviation, the additional losses occurring in the iron guide rail cannot be neglected at this operation point. To analyse this phenomenon, an FEM simulation is performed with primary and secondary windings powered by 10 A in opposite direction, which represents the ideal short-circuit operation of a transformer. From Figure 2 it can be taken that the flux no longer penetrates the soft-ferrite actuator only, but also the iron guide rail between the yokes of the

primary actuator. The mean values of the flux density in the primary actuator and the iron between the yokes are respectively 0.021 T and 0.016 T. The latter determines the additional losses occurring in the guide rail. At this operation point, the CPS has a high percentage of primary side leakage flux $\Phi_{\sigma,1}$.

To analyse the influence of the current in the windings, FEM simulations for various primary winding currents at no-load and short-circuit operation are performed. Furthermore, an iron ring of the same material as the guide rail is measured at f_{CPS} = 25 kHz to identify the relationship between the magnitude of the flux density in the material and its loss density. The simulation and measurement results are presented consecutively in Figure 3 and 4. From Figure 3 can be concluded that the flux density in the iron between the yokes of the primary actuator B_{Rail} is linearly dependant to the primary winding current I_p and the load of the CPS system. Furthermore in Figure 4 can be seen, that the loss density in iron increases quadratically with the flux density. At the maximum primary current of 10 A at short-circuit operation, the flux density reaches 0.16 T, which leads to the loss density of 17 W/kg. The maximum loss density of the actuators is 1.7 W/kg. Considering the weight of the actuators, the maximum loss of both actuators is 0.8 W. The sum of the resistances of both windings is 94 mΩ. Assuming the maximum current flow of 10 A in both windings, the maximum ohmic loss in the windings is 9.4 W. The CPS system is designed to be able to transmit power of 250 W at its working point. Without the additional losses considered, the constructed CPS system should have an efficiency of more than 95% at its working point. In [3] is shown, that the CPS system only could reach a maximum efficiency of 53% at its working point. Therefore, the additional losses cannot be neglected.

The linear dependency of the flux density in the guide rail B_{Rail} on the primary current I_p in Figure 3 is based on the assumption of constant inductances. In the reality it also depends on other factors, such as saturation, eddy currents and hysteresis losses [4].

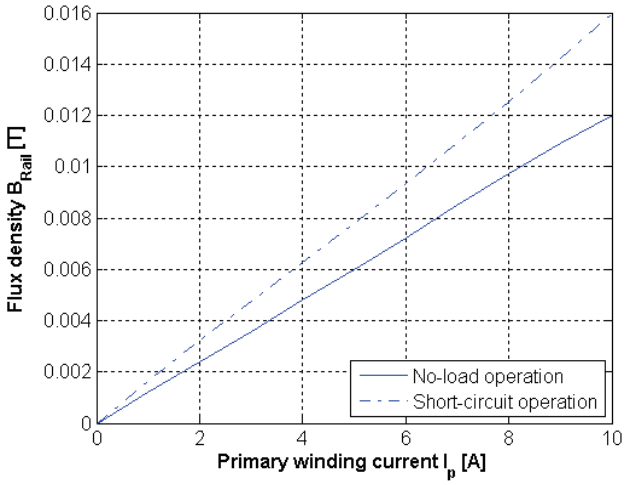

Fig. 3. Mean value of magnetic flux density between the yokes of the primary actuator B_{Rail} as a function of primary current I_p

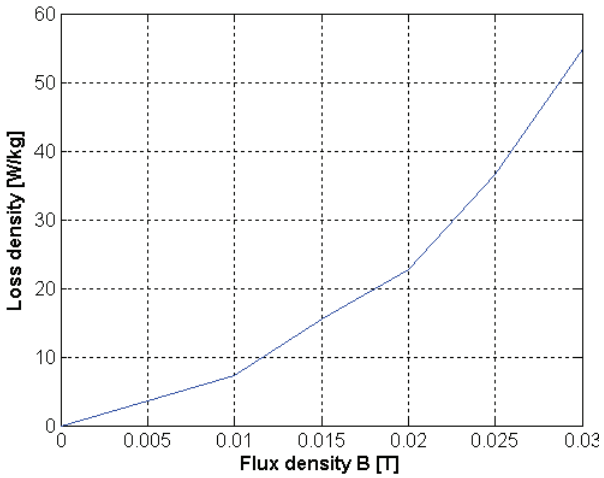

Fig. 4. Loss density of the guide rail material as a function of flux density B

Due to the non-uniform distribution of the flux density, it is complicated to determine the exact value of the losses in the guide rail. An experimental method to model an integrated CPS system with consideration of the additional non-linear losses will be introduced in the next section.

3. Modelling approaches

In the next subsections the classic equivalent circuit of a CPS system will be presented and the proposed extended model will be introduced.

3.1. The equivalent circuit of a CPS system

In Figure 5 a classical equivalent circuit model based on mutual inductances of the constructed CPS system is presented. U_1 and U_2 represent input and output voltage of the CPS system respectively. I_1 and I_2 are the input and output currents and I_p and I_s are the currents in primary and secondary winding respectively. R_p and R_s are the resistances of the primary and secondary winding. The inductance matrix **L** describes the behaviour of the system without additional losses according to (1). The parallel capacitances C_p and C_s compensate the reactive power required for the power transmission. Therefore, at the input of the CPS only active power is needed [5]. The load connected to the output is a rectifier and a battery, which is assumed as a purely resistive load R_{Load}.

In the previous section is mentioned, that the primary side leakage flux is a function of primary current and the load of the CPS system, which is represented by the secondary winding current. In an operating CPS the ratio of primary and secondary current is determined by its reflected impedance $\underline{Z}_r$. The reflected impedance $\underline{Z}_r$ depends on the secondary compensation and for the constructed CPS applies [6]:

$$\underline{Z}_r = \frac{-j\omega M i_s}{i_p} = \left(\frac{M}{L_s}\right)^2 R_{\text{Load}} - j\omega\frac{M^2}{L_s}. \tag{2}$$

If the inductance matrix of the CPS is unchanged, the dependency is limited to the load impedance R_{Load}, or in this case to the battery inner resistance. Considering the behaviour of the additional losses, beside the inductance matrix the circuit model of the CPS should consist of at least two additional elements: leakage inductance $L_{\sigma Fe}$, to model the increasing leakage flux, and iron resistance $R_{\sigma Fe}$, to model the losses in the system. Both elements are connected in series and a function of primary current I_p and load resistance R_{Load}.

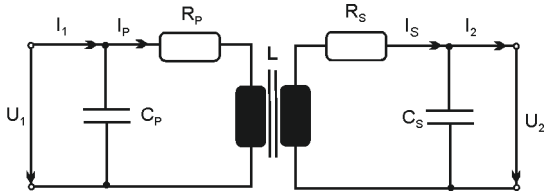

Fig. 5. A classic equivalent circuit of a CPS system with parallel compensation on both primary and secondary sides

3.2. Proposed extended equivalent circuits of the constructed CPS system

The next step is to determine a feasible model for the CPS. This can be conducted using measurement of an uncompensated CPS system at various primary winding currents I_p and load resistances R_{Load}. The results are compared with the analytical equations of the proposed equivalent circuits. To simplify the analytical equation, the proposed additional circuit elements $R_{\sigma Fe}$ and $L_{\sigma Fe}$ are combined to a single complex impedance $\underline{Z}_{\sigma Fe}$. The physical behaviour of this impedance is initially not defined. Three possibilities to arrange the additional impedance $\underline{Z}_{\sigma Fe}$ in an equivalent circuit model of the CPS are proposed: on the primary side, on the secondary side, and on both sides. In Figure 6 the three possible models are presented respectively.

The following quantities are determined from measurements: the primary voltage U_1, the primary winding current I_p and its phase shift φ_1. With these parameters the input impedance of the CPS can be determined with the equations:

$$\text{Re}\{\underline{Z}_{in}\} = \frac{U_1}{I_p}\cos\varphi_1 \quad \text{and} \quad \text{Im}\{\underline{Z}_{in}\} = \frac{U_1}{I_p}\sin\varphi_1. \tag{3}$$

The general equations of the proposed extended circuit model can be determined using the model in Figure 6c. In case of the model in Figure 6a and Figure 6b the additional impedance $\underline{Z}_{\sigma Fe}$ in the secondary or primary side can be set to zero respectively. The general analytical equations can be defined with the secondary input impedance $\underline{Z}_{in,\,2}$, the reflected impedance $\underline{Z}_r$ and the input impedance of the CPS system $\underline{Z}_{in}$. The general mathematical equations are [7]:

$$\underline{Z}_{in,2} = j\omega L_s + R_s + \underline{Z}_{\sigma FeS} + R_{\text{Load}}, \tag{4}$$

$$\underline{Z}_r = \frac{(\omega M)^2}{\underline{Z}_{in,2}}, \text{ and} \tag{5}$$

$$\underline{Z}_{in} = j\omega L_p + R_p + \underline{Z}_{\sigma FeP} + \underline{Z}_r. \tag{6}$$

Through separation of real and imaginary component of (6), the value of the additional impedances $\underline{Z}_{\sigma Fe}$ for diverse primary currents I_p and load resistances R_{Load} can be calculated. In the next step, measurements of a compensated CPS system with various primary winding currents I_p are performed and the results are compared to the simulation. To validate the robustness of the model, the air gap between the primary and secondary actuators is varied, which represents variation of the inductance matrix **L**. The compared parameters are output power and efficiency of the CPS system.

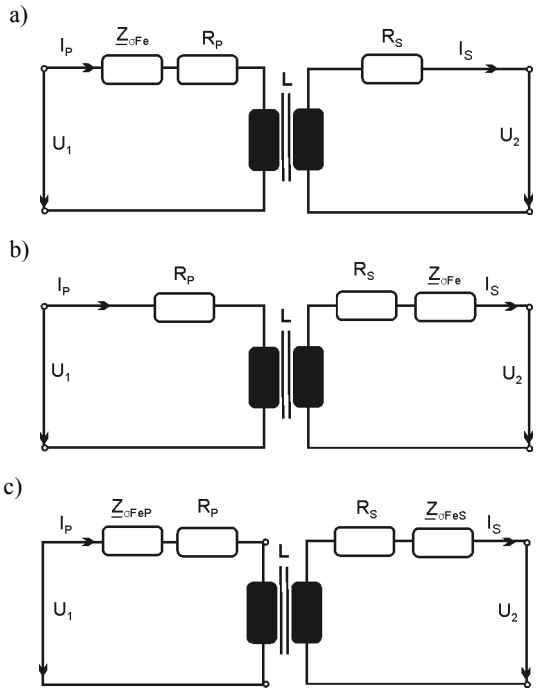

Fig. 6. Proposed extended equivalent circuit models with additional impedances $\underline{Z}_{\sigma Fe}$ a) on primary side, b) on secondary side, c) on primary and secondary sides

4. Results

From the three possibilities of the extended equivalent circuit model of the CPS, the model with the additional circuit elements arranged on the primary side (Fig. 6a) shows the most feasible results. The dependency of the impedance on the primary current I_p and the load im-

pedance R_{Load} shows a consistent characteristic. The simulations with the compensated CPS show a good accordance to the measurements. The maximum deviation of the output power P_{out} and the efficiency η are 10.9% and 14.3% respectively. This occurs at a distance of primary and secondary actuator d = 2 mm and a load resistance R_{Load} = 10 Ω. At its designed position and load resistance, the deviation of the output power and efficiency are 6.5% and 4.9% respectively. In the model with the additional elements on the secondary side of the CPS (Fig. 6b), the imaginary part of the impedance $\underline{Z}_{\sigma Fe}$ is negative at every working points except for short-circuit operation and the real part becomes negative at a load resistance R_{Load} = 10 Ω. This is physically not plausible for an inductive energy transmission, since the losses caused by the leakage flux is unlikely capacitive and a negative resistance are not applicable for the loss modelling. In the model with additional elements on both sides of the CPS (Fig. 6c), the impedances become purely ohmic and the variation of the leakage inductance is not modelled. In the short-circuit operation the additional primary resistance is also negative and in the simulation with the compensated CPS the output power and efficiency are much lower than the measurement results. At its designed position and load resistance, the deviation of the output power and efficiency reaches 51% and 56% respectively. Therewith the model in Figure 6c is considered as not plausible.

In Figure 7 the extended equivalent circuit of the constructed CPS system is shown. The additional elements on the primary side are the leakage inductance of the guide rail $L_{\sigma Fe}(I_p, R_{\mathrm{Load}})$ and its iron resistance $R_{\sigma Fe}(I_p, R_{\mathrm{Load}})$. It is assumed, that the fluctuation of the battery internal resistance is limited between half and twice of its nominal value. The variation of this resistance results in a change of the primary and secondary winding current ratio I_p/I_s, which influences the variation of the leakage flux $\Phi_{\sigma,1}$. The change of the load resistance R_{Load} is proportional to the current ratio I_p/I_s.

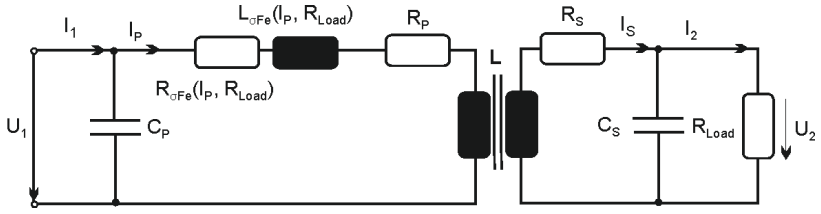

Fig. 7. An extended equivalent circuit of an integrated CPS system with parallel compensation on both primary and secondary side

Figure 8 shows $L_{\sigma Fe}$ and $R_{\sigma Fe}$ as a two dimensional function of the current through the primary winding I_p and fraction of the load resistance R_{Load} for the chosen equivalent circuit model. Both additional elements $L_{\sigma Fe}$ and $R_{\sigma Fe}$ increase proportional to I_p until their saturation points at I_p = 2 A. The leakage inductance $L_{\sigma Fe}$ has no remarkable load dependency and the iron resistance $R_{\sigma Fe}$, which represents the losses in the guide rail, is inversely proportional to the load resistance R_{Load}. The values of these elements are interpolated for the complete simulation range and built in the simulation model as two dimensional lookup-tables.

In Figure 9 the deviation between measurement and simulation results is presented. The calculation of the deviation is normalised to the measurement results. The input variable of the

simulation is the primary current I_1, which values are obtained from the measurements. Figure 9a shows the deviation of the output power P_{out} and Figure 9b the deviation of the efficiency η. The the quantities depend on the load resistance R_{Load} and the distance between primary and secondary actuators d. In Figure 9a can be seen, that the characteristic of the deviation of the output power P_{out} can be divided in two sections: the working points below and above the nominal load resistance. At a load resistance R_{Load} smaller than its nominal value, the deviation reaches its minimum at the nominal distance of the CPS. If the load resistance R_{Load} rises above its nominal value, the deviation declines with increasing distance d. In Figure 9b can be recognized, that the deviation of the efficiency η increases

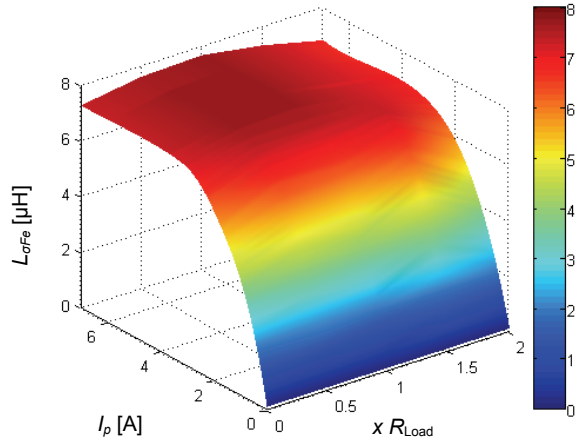

Fig. 8a. Additional leakage inductance $L_{\sigma Fe}$ to model the losses in the guide rail as a function of primary winding current I_p and load resistance R_{Load}

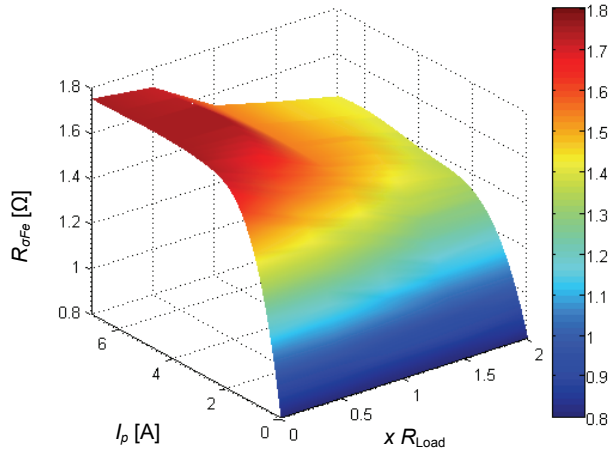

Fig. 8b. Additional iron losses $R_{\sigma Fe}$ to model the losses in the guide rail as a function of primary winding current I_p and load resistance R_{Load}

proportional to the load resistance R_{Load}. At its nominal position, the deviation of the efficiency η is small compared to other positions.

The deviation between measurement and simulation can be related to the measurement accuracy of the CPS in the determination of the additional impedance $\underline{Z}_{\sigma Fe}$. This impedance depends on the condition and environment of the CPS. Furthermore, the non-ideal current supply of the test bench is not modelled in the simulation. It also contributes to the deviation of the simulation results.

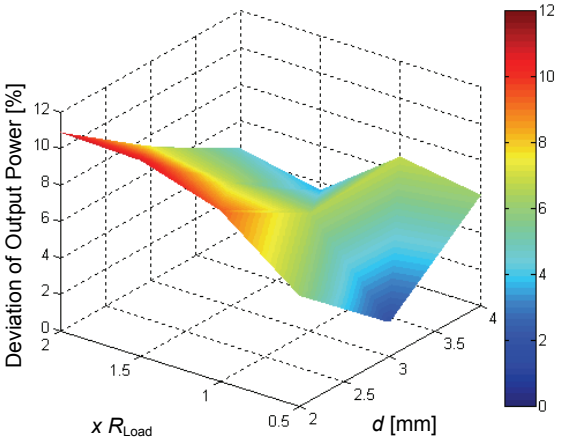

Fig. 9a. Deviation between measured and simulated output power P_{out}

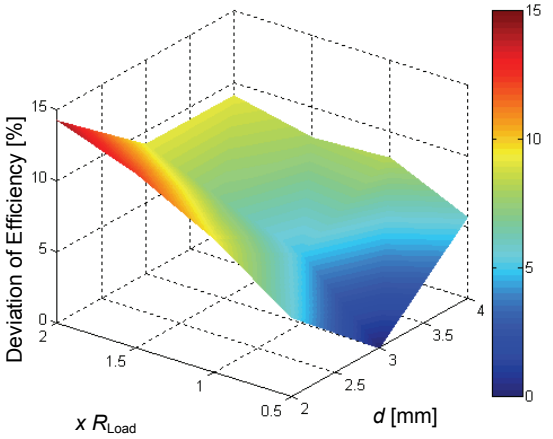

Fig. 9b. Deviation between measured and simulated efficiency η

5. Conclusions

In this paper an extended equivalent circuit model of a CPS to model additional iron losses in the guide rail using discrete circuit elements has been introduced. Through measurement of

an uncompensated CPS system with various primary winding currents I_p and load resistances R_{Load}, the behaviour of the elements and the configuration of the extended equivalent circuit model are determined. The additional components are a leakage inductance $L_{\sigma Fe}$ and an iron resistance $R_{\sigma Fe}$, which are connected in series and placed on the primary side of the CPS. Both depend on the primary winding current I_p and the load resistance R_{Load} of the CPS system. The leakage inductance $L_{\sigma Fe}$ represents the increasing leakage flux and the iron resistance $R_{\sigma Fe}$ represents the losses in the system. These elements are integrated in the simulation model through application of two dimensional lookup-tables. The extended model is validated through measurement and simulation of a compensated CPS system at various working points. The considered variations are the air gap distance between primary and secondary actuators and the battery internal resistance. During operation, the relative position of the actuators can be different from its reference value, since slight deviation in the MGS of the elevator car can occur [8]. The value of the battery internal resistance depends on its environment, such as temperature, age and state of charge. The simulation and measurement results show a good accordance with an output power P_{out} and efficiency η deviation at its working point of 6.5% and 4.9% respectively. The modelling accuracy of the CPS is thereby increased.

References

[1] Lee J.-Y., Lee I.-J., Kim J.-W. et al., *Contactless power transfer system combined with linear electric machine.* Proc. 8th International Conference on Electrical Machines and Systems (ICEMS), Seoul, Korea, pp. 1544-1548 (2007).

[2] Appunn R., Riemer B., Hameyer K., *Contactless power supply for magnetically levitated elevator systems.* Proc. 20th International Conference on Electrical Machines (ICEM), Marseille, France, pp. 600-605 (2012).

[3] Appunn R., Putri A.K., Hameyer K., *Design of a contactless power supply for magnetically levitated elevator systems integrated into the guide rail.* Applied Mechanics and Materials 416(417): 333-338 (2013).

[4] Ranta M., Hinkkanen M., Belahcen A., Luomi J., *Inclusion of hysteresis and eddy current losses in non-linear time-domain inductance model*. Proc. 37th Annual Conference on IEEE Industrial Electronics Society (IECON), Melbourne, Australia, pp. 1897-1902 (2011).

[5] Stielau O.H., Covic G.A., *Design of loosely coupled inductive power transfer systems.* Proc. International Conference on Power System Technology (PowerCon), Perth, Australia 1: 85-90 (2000).

[6] Wang C.-S., Stielau O.H., Covic G.A., *Load models and their application in the design of loosely coupled inductive power transfer systems.* Proc. International Conference on Power System Technology (PowerCon), Perth, Australia 2: 1053-1058 (2000).

[7] Wang C.-S., Covic G.A., Stielau O.H., *General stability criterions for zero phase angle controlled loosely coupled inductive power transfer systems.* Proc. 27th Annual Conference of the IEEE Industrial Electronics Society, Denver, USA 2: 1049-1054 (2001).

[8] Schmülling B., Appunn R., Wikullil F., Hameyer K., *Design and operation of an electromagnetically guided elevator test bench.* Proc. 7th International Symposium on Linear Drives for Industry Applications (LDIA), Incheon, Korea, pp. 114-115 (2009).